 https://doi.org/10.3311/PPee.24770

Periodica Polytechnica Electrical Engineering and Computer Science, 68(3), pp. 240–245, 2024

Photovoltaic Microinverter Based on Buck-Boost Converter and Discharge Circuit

Mohammed El Bachir Ghribi[1*], Zine Eddine Touhami Ternifi[2], Ghalem Bachir[2], Michel Aillerie[3]

[1] Applied Power Electronics Laboratory (LEPA), Department of Electrical Engineering, Faculty of Electrical Engineering, University of Sciences and Technology of Oran, Bir El Djir, P.O.B. 1505, El-Mnaouer, 31000, Oran, Algeria
[2] Laboratory of Sustainable Development of the Electrical Energy (LDDEE), Department of Electrical Engineering, Faculty of Electrical Engineering, University of Sciences and Technology of Oran, Bir El Djir, P.O.B. 1505, El-Mnaouer, 31000, Oran, Algeri
[3] Laboratoire Matériaux Optiques, Photonique et Systèmes (LMOPS), CentraleSupélec, Université de Lorraine, 2 rue E. Belin, P.O.B. 57070, F-57000, Metz, France
[*] Corresponding author, e-mail: mohammedelbachir.ghribi@univ-usto.dz

Received: 01 January 2024, Accepted: 12 June 2024, Published online: 20 June 2024

Abstract

This paper presents a novel topology for photovoltaic microinverters that uses a buck-boost converter coupled with a discharge circuit. The system enables efficient conversion of electrical energy from the solar panel without requiring voltage filters or step-up transformers. For its control, an exponential action control strategy is used, as it allows effective tracking of the reference voltage. The stability of the overall control and inverter system is demonstrated and detailed using the Lyapunov method. The sizing of the components used is also detailed. The performance of this topology is evaluated under various load conditions, revealing low harmonic distortion (THD) in both current and voltage, with the best THD of 1% being obtained at a power factor of 0.8. This makes it a promising solution for photovoltaic energy conversion.

Keywords

micro-inverter, Buck-Boost, discharge circuit, Lyapunov

1 Introduction

Microinverters have emerged as an innovative solution to maximize the efficiency and performance of solar energy systems by directly converting the direct current generated by each solar panel into alternating current. There are different microinverter configurations that offer excellent performance but come with complex or challenging control and a significant number of components [1, 2]. To achieve better performance with fewer components, researchers have explored the use of multi-stage microinverters. The first stage of these microinverters is a DC-DC converter, which preconditions the voltage and current waveforms provided by the photovoltaic source, the primary types of converters used are boost converters as they provide an amplified output voltage [3–7]. Depending on the requirements, other converters such as buck or flyback converters are employed [8–10].

We propose a new topology based on the symmetric boost-discharge circuit [11], but utilizing a buck-boost converter [12, 13]. The goal is to have a high-performance converter using a reduced number of components capable of delivering standardized voltage without the need for a voltage step-up transformer. The buck-boost converter is coupled with a discharge circuit, and the symmetric operation of the two structures enables the generation of a voltage waveform resembling a rectified sine wave. Once this waveform is obtained, it is straightforward to obtain the second half-cycle to achieve sinusoidal voltages and currents.

This paper aims to introduce the new structure, provide a comprehensive circuit modeling, describe a method for sizing the various active components used, and present the control strategy for generating the desired voltage waveform. We conclude with the presentation of all simulation results.

2 The Proposed Topology and its Control

This topology consists of three cascaded circuits as shown in Fig. 1. The first circuit is a buck-boost converter responsible for increasing the voltage by charging capacitor C2. The second circuit is a discharge circuit for capacitor C2, placed in parallel with it, which allows for a decrease in voltage. Both

Cite this article as: Ghribi, M. E. B., Ternifi, Z. E. T., Bachir, G., Aillerie, M. "Photovoltaic Microinverter Based on Buck-Boost Converter and Discharge Circuit", Periodica Polytechnica Electrical Engineering and Computer Science, 68(3), pp. 240–245, 2024. https://doi.org/10.3311/PPee.24770

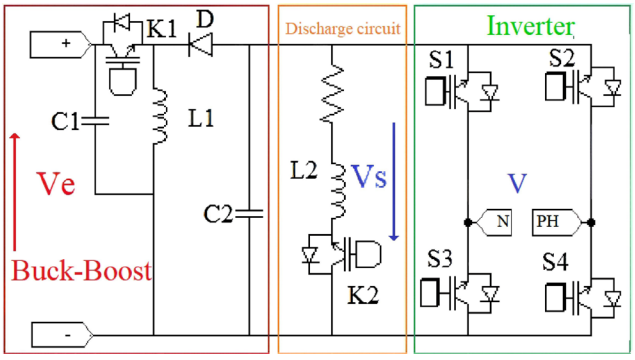

Fig. 1 Diagram of the Proposed Topology

the switches in the buck-boost converter and the discharge circuit operate symmetrically, enabling the creation of a rectified sinusoidal waveform. The third circuit is an inverter bridge that reverses the waveform obtained during the second half-cycle. This results in generating a sinusoidal waveform.

2.1 Modeling of the Buck-Boost Converter Coupled with the Discharge Circuit

The modeling of the buck-boost converter and the discharge circuit relies on the use of a Boolean variable S to account for the state of switches K1 and K2. When the switches are closed, S takes the value of 1. Conversely, when the switches are open, S takes the value of 0. It is important to note that, by definition, S also represents the state of the control signal.

Phase 1

When the power switches are open (S=0) as shown in Fig. 2(a), capacitor C1 charges from the solar panel. Inductance L2, on the other hand, is responsible for charging capacitor C2 and supplying energy to the load.

$$\begin{aligned} \frac{dI_{L1}}{dt} &= -\frac{V_s}{L_1} \\ \frac{dI_{L2}}{dt} &= 0 \\ \frac{dV_s}{dt} &= \frac{I_{L1}}{C2} - \frac{V_s}{R \cdot C2} \end{aligned} \tag{1}$$

Phase 2

When the switches are closed (S=1) as shown in Fig. 2(b), capacitor C1, as well as the solar panel, charge inductor L1. Capacitor C2, on the other hand, discharges through the load and the discharge circuit.

$$\begin{aligned} \frac{dI_{L1}}{dt} &= \frac{V_e}{L_1} \\ \frac{dI_{L2}}{dt} &= \frac{V_s}{L_2} \\ \frac{dV_s}{dt} &= -\frac{I_{L2}}{C2} - \frac{V_s}{R \cdot C2} \end{aligned} \tag{2}$$

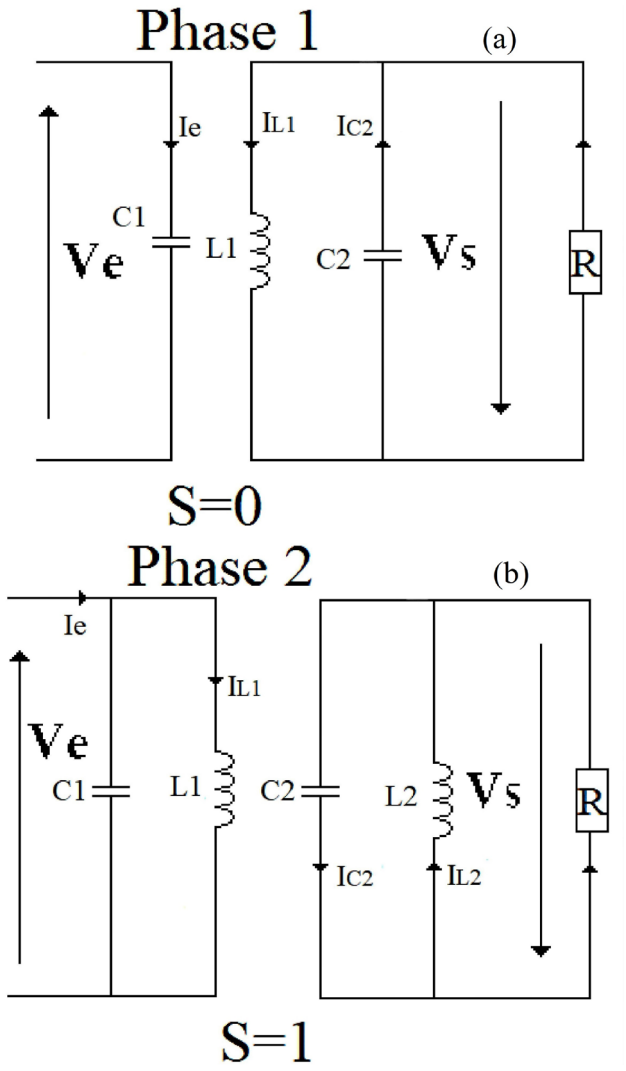

Fig. 2 Equivalent Circuit Diagram of the Buck-Boost Converter with the Discharge Circuit, (a) Phase 1 where the switch is off, (b) Phase 2 where the switch is on.

With the introduction of the switch state variable, the system modeling results in a third-order state representation that switches between two states. This transition from one state to another is facilitated by the switching of the switches and, consequently, by the variable 'S'.

$$\frac{d}{dt}\begin{bmatrix} I_{L1} \\ I_{L2} \\ V_s \end{bmatrix} = \begin{bmatrix} 0 & 0 & \frac{S-1}{L_1} \\ 0 & 0 & \frac{S}{L_2} \\ \frac{1-S}{C2} & \frac{-S}{C2} & \frac{-1}{R \cdot C2} \end{bmatrix} \cdot \begin{bmatrix} I_{L1} \\ I_{L2} \\ V_s \end{bmatrix} + \begin{bmatrix} \frac{S}{L_1} \\ 0 \\ 0 \end{bmatrix} V_e \tag{3}$$

2.2 Sizing of the micro-inverter

The sizing is performed to directly provide a sinusoidal voltage of 225 V and a maximum power of 300 W. The panel delivers its maximum power at a voltage of 36 V under nominal conditions. To simplify the calculations,

each component value is determined independently of the others, which may result in approximate results.

The expression for the current ripple of the inductance in a buck-boost converter is used to determine the input inductance [11].

$$L_1 = \frac{V_s}{\Delta I_{L_1}} \approx \frac{V_{e-\max} V_{s-\max}}{4 \cdot \Delta I_{L_1} \cdot f_s \left(V_{e-\max} + V_{s-\max}\right)} \tag{4}$$

$$C2_{\max} = \frac{I_{c2} \Delta t}{\Delta V} \approx \frac{I_{c2}}{4 \cdot \Delta V \cdot f_s} \tag{5}$$

$$\frac{\varepsilon_p}{I_{L2-\max} \cdot f_{com-\min}} < L_2 < \frac{V_{s-\max}}{I_{L2-\max} \cdot f_{com-\min}} \tag{6}$$

The output voltage waveform depends on the absorbed current, which is typically limited for a solar panel. The purpose of an input capacitor is to smooth the voltage and provide current during high power demands. This capacitor is assumed to be equal to the C2 capacitance of the converter.

2.3 Control and stability

We have chosen to use exponential control for our system. This control is based on the fact that the control signal is exponential with respect to the error, allowing for a more dynamic switch state change. This state change is only limited by the maximum switching frequency of the switch, and the switching frequency varies over a period.

$$\varepsilon_p = V_{ref} - V_S \tag{7}$$

$$S = step\left(|\varepsilon|^n - k\right) \tag{8}$$

The peculiarity of using the absolute value is that it introduces a permanent error into the control. The reference voltage added to this permanent error forms a threshold at which the control switches and changes the state of switches K1 and K2. Thanks to the absolute value of the error, the output voltage is always higher than the reference voltage.

$$\varepsilon_p = \sqrt[n]{k}, \quad n > 1 \tag{9}$$

$$V_s = \sqrt{\left(\frac{V^2_{ref-\max}}{2} + \frac{4}{\pi} \varepsilon_p \cdot V_{ref-\max} + {\varepsilon_p}^2\right)} \tag{10}$$

The Lyapunov method is used to determine the stability of an equilibrium point or motion of a system using an energy function, typically a quadratic function. In the current case, this method is applied to a nonlinear system that switches between two states [14–17].

For a system to be stable, the Lyapunov function must be zero at the origin, and it is defined in such a way that it is always strictly positive and its derivative is strictly negative. In other words, the Lyapunov function must decrease at each iteration and reach a minimum when the system reaches its equilibrium point.

By using this method, one can determine the phases of stability and instability of the system.

$$\varepsilon_1 = |\varepsilon| - \sqrt[n]{k}; \quad v(\varepsilon_1) = \frac{\varepsilon_1^2}{2} \tag{11}$$

$$\varepsilon < 0 \rightarrow \varepsilon_1 = -\varepsilon - \sqrt[n]{k} \rightarrow \varepsilon_1' = -V_s' \tag{12}$$

$$\varepsilon > 0 \rightarrow \varepsilon_1 = \varepsilon - \sqrt[n]{k} \rightarrow \varepsilon_1' = V_s' \tag{13}$$

Phase 1

$$-\sqrt[n]{k} < \varepsilon < 0 \rightarrow -\sqrt[n]{k} < \varepsilon_1 < 0 \rightarrow S = 0 \tag{14}$$

The switches are open (S=0), and the capacitor is charging thanks to the energy stored in the coil L1. The voltage across the capacitor increases, so from Eq. (12), we find:

$$V_s' > 0 \rightarrow \varepsilon_1' > 0 \tag{15}$$

Phase 2

$$\varepsilon < -\sqrt[n]{k} \rightarrow \varepsilon_1 > 0 \rightarrow S = 1 \tag{16}$$

When the buck-boost switch is closed (S=1), capacitor C2 discharges, resulting in a decrease in voltage across the load. From Eqs. (11) and (12), we find:

$$V_s' < 0 \rightarrow \varepsilon_1' < 0 \tag{17}$$

The Lyapunov function is zero for the initial conditions, it is strictly positive, and its derivative is strictly negative. For phases one and two, the conditions are met, and the system is asymptotically stable and attractive, as shown in Fig. 3.

$$\begin{aligned} &V(0) = 0 \\ &V(\varepsilon_1) = \frac{\varepsilon_1^2}{2}, \quad \varepsilon_1 \neq 0 \\ &V'(\varepsilon_1) = \varepsilon_1 \dot{\varepsilon}_1 < 0 \end{aligned} \tag{18}$$

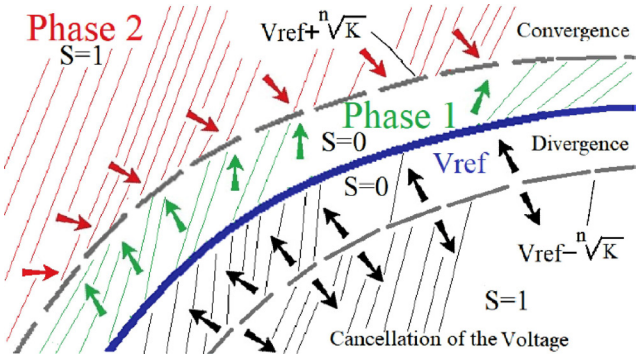

Fig. 3 Phases of stability

In the case where the output voltage is lower than the reference voltage minus the permanent error, switch K1 remains open for the remainder of the half-cycle, and the buck-boost voltage becomes zero. This case can occur for low switching frequencies or an undersized power source.

Eqs. (19) and (20) demonstrate that when V_s is less than V_{ref}, the system becomes unstable. So, the system converges towards the switching line $V_{ref} + \sqrt[n]{k}$ and diverges from the switching line $V_{ref} - \sqrt[n]{k}$.

$$0 < \varepsilon < \sqrt[n]{k} \rightarrow -\sqrt[n]{k} < \varepsilon_1 < 0 \rightarrow S = 0 \rightarrow V_s' > 0 \rightarrow \varepsilon_1' < 0 \rightarrow V'(\varepsilon_1) > 0 \quad (19)$$

$$\sqrt[n]{k} < \varepsilon \rightarrow -\sqrt[n]{k} < \varepsilon_1 > 0 \rightarrow S = 1 \rightarrow V_s' < 0 \rightarrow \varepsilon_1' > 0 \rightarrow V'(\varepsilon_1) > 0 \quad (20)$$

This control method does not enable tracking of the maximum power point. Under nominal conditions, the panel delivers its maximum power whenever K1 is closed and provides a low power to charge C1 when K1 is open. Therefore, the maximum power that the panel can deliver is directly dependent on the duty cycle of the buck-boost, as shown in Eq. (21). Theoretically, for this particular case, the converter is capable of transmitting 90.25% of the total power produced by the PV panel.

$$P_{\max} = \alpha \cdot P_{pv-\max} \approx \frac{V_{s-\max}}{V_{e-\max} + V_{s-\max}} P_{pv-\max} \quad (21)$$

A significant portion of the losses is caused by the discharge circuit, and these losses are denoted by Eq. (22).

$$P_{disc} = \frac{2}{T} \int_0^{\frac{T}{2}} |V_s(t)| I_{L2}(t) \cdot dt \quad (22)$$

3 Simulation results

For the simulation, the reference voltage is defined as $\boldsymbol{V_{ref} = 315 \cdot \sin(2\pi \cdot 50\, t)}$ which results in an effective value of 222.6 V. The permanent error is chosen as $\boldsymbol{\varepsilon_p = 1.4\ V}$. The theoretical offset between the reference voltage and the actual output voltage of the inverter is thus approximately 224 V.

The simulation demonstrates that the system perfectly tracks the voltage reference, as shown in Fig. 4. Indeed, the effective output voltage is always higher than the reference voltage, and Table 1 indicates that the difference between these two voltages is 3.4 V.

Regarding the discharge current, it reaches its maximum level when capacitor C2 needs to discharge completely. This situation is clearly observed in Fig. 4, where the peak always occurs at the end of the half-cycle. The use of a discharge inductance serves to prevent rapid discharge by limiting the frequency at which the switches make their transitions. Therefore, the increase in the discharge current is equivalent to a second-order response.

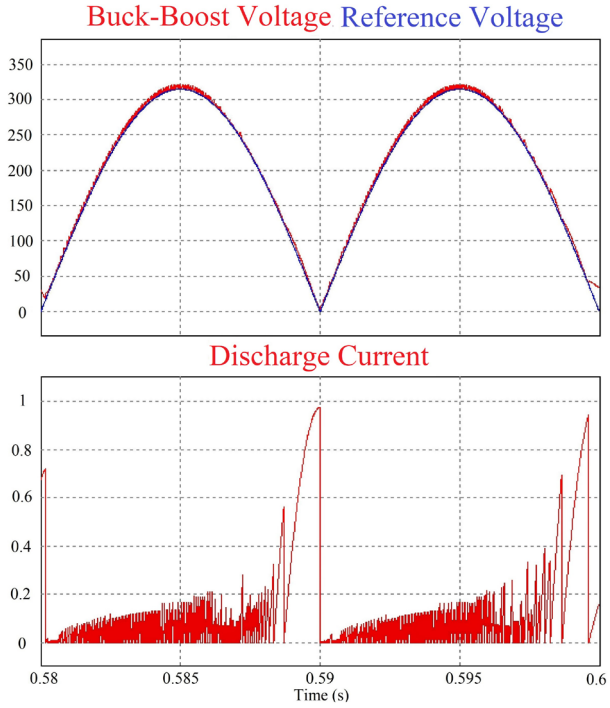

Fig. 4 Output Voltage of the Buck-Boost and Discharge Current

Table 1 Average value of the discharge current and RMS of the inverter voltage of the Fig. 4

	RMS	Value Average
Buck-boost voltage	226 V	205 V
Voltage reference	222.2 V	200 V
Discharge current	//	0.137 A

The simulation allows us to estimate an efficiency of 89%, with a significant portion of the losses caused by the discharge of excess charge stored in the capacitor, primarily at the end of each half-cycle. In the nominal case, this loss is estimated to be 18 W, as shown in Eq. (22).

The test with a purely resistive load shows a sinusoidal output voltage, as indicated in Fig. 5, and the voltage and current THD is only 2.2%, as shown in Table 2. For a purely inductive load, zero crossing is more difficult, as shown in Fig. 6. The voltage THD increases to 3.3%, but the current THD decreases. However, the offset between the effective value of the output voltage and the reference voltage increases from 3 V to 4.5 V, as shown in Table 3. The theoretical offset is only 1.3 V. This difference is due to a combination of factors, with the main one being that, at t = {0,T/2}, the voltage is higher than the calculated $\boldsymbol{\varepsilon_p}$, ranging from 2 to 4 V.

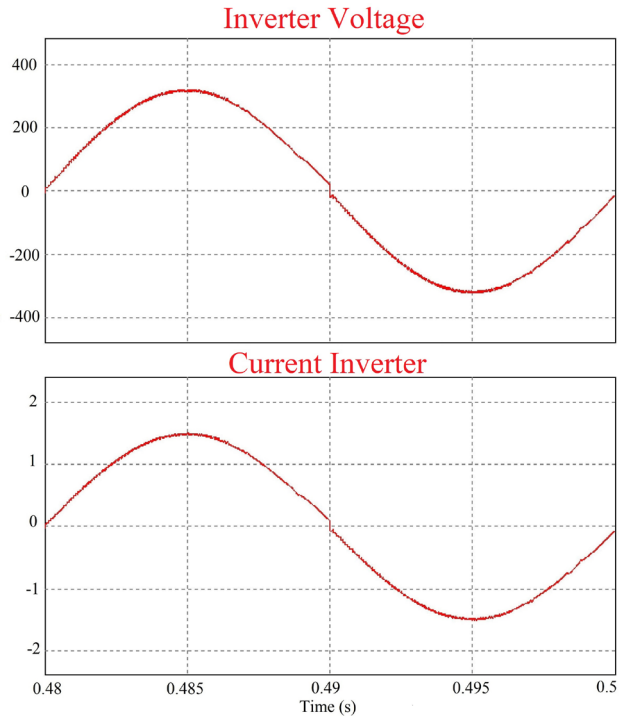

Fig. 5 Voltage and Current of the Inverter for a Highly Restrictive Load

Table 2 RMS and THD of inverter current and voltage in Fig. 5

	RMS	THD 50 Hz
Inverter Voltage	226 V	2.2%
Inverter Current	1.06 A	2.15%

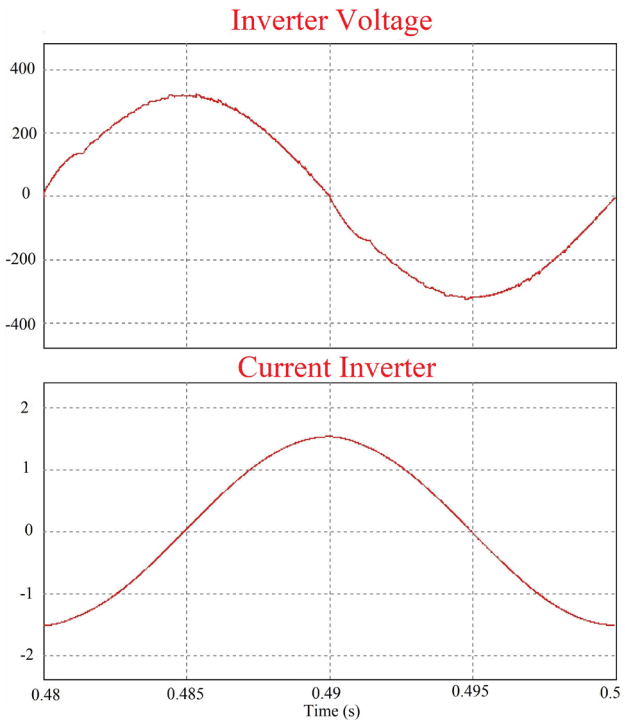

Fig. 6 Voltage and Current of the Inverter for a Highly Inductive Load

Table 3 RMS and THD of inverter current and voltage in Fig. 6

	RMS	THD 50 Hz
Inverter Voltage	227.5 V	3.3%
Inverter Current	1.06 A	1.46%

Figs. 7 and 8 show the variation of the Total Harmonic Distortion (THD) of current and voltage as a function of the load factor. It can be observed that THD is minimal for a

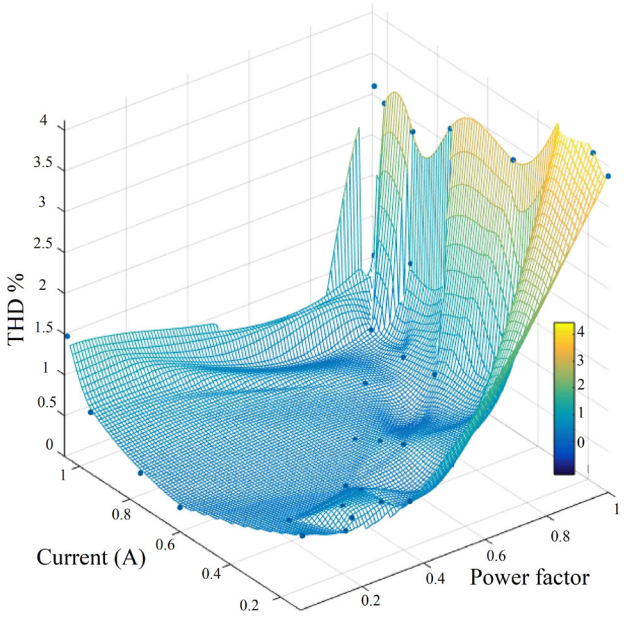

Fig. 7 THD of Current as a Function of its Intensity and Power Factor

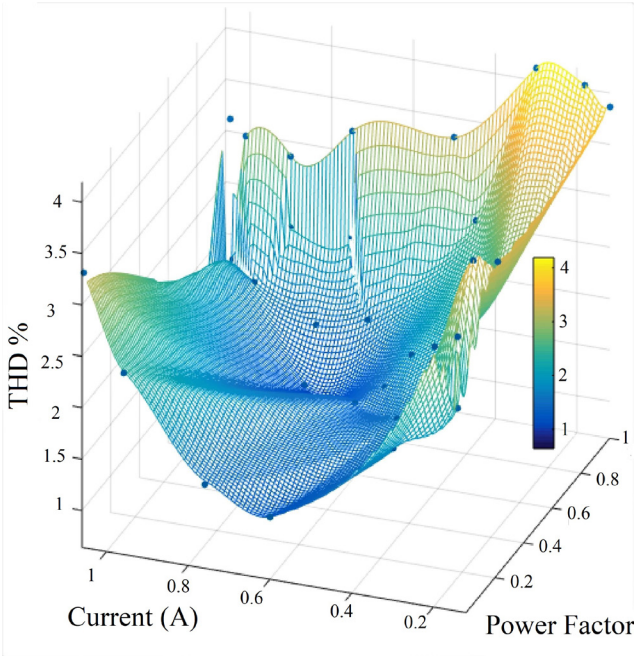

Fig. 8 THD of Voltage as a Function of its Intensity and Power Factor

power factor of 0.8. The THD of voltage reaches a minimum of 1%, while the THD of current reaches a minimum of 0.5%.

The variation of THD of current is exponential within the power factor range between 0.8 and 1. When the power factor goes from 0.8 to unity, the Total Harmonic Distortion (THD) increases from 0.5% to 3.5%.

4 Conclusion

This new topology offers good overall performance using a reduced number of components, only 2 high-frequency switches and 4 low-frequency ones, without the need for a voltage filter or electrical transformer. The average switching frequency of the high-frequency switches is less than 10 kHz, with peaks and minima varying depending on the generated power and the nature of the load. The maximum instantaneous peak is limited by the control to 20 kHz. This inverter provides a high-quality sinusoidal voltage with a voltage THD of 2% under nominal operation. In the studied cases, the converter is capable of supplying up to 90% of the maximum solar panel power.

References

[1] Marangalu, M. G., Kurdkandi, N. V., Alavi, P., Khadem, S., Tarzamni, H., Mehrizi-Sani, A. "A New Single DC Source Five-Level Boost Inverter Applicable to Grid-Tied Systems", IEEE Access, 11, pp. 24112–24127, 2023. https://doi.org/10.1109/ACCESS.2023.3253806

[2] Farkas, B., Veszprémi, K. "Design of HIL for multi-level inverter using Zynq–7000 platform – Part 1", Periodica Polytechnica Electrical Engineering and Computer Science, 61(3), pp. 264–271, 2017. https://doi.org/10.3311/PPee.10902

[3] Qasim, M. A., Ivanovich Velkin, V., Mohammed, M. F., Ahmad Sammour, A., Du, Y., Abdul-Adheem Salih, S., Abdulkareem Aljashaami, B., Parviz Gulmurodovich, S. "Design of a multi-level inverter for solar power systems with a variable number of levels technique", International Journal of Power Electronics and Drive Systems (IJPEDS), 14(2), pp. 1218–1229, 2023. http://doi.org/10.11591/ijpeds.v14.i2.pp1218-1229

[4] Ternifi, T., Bachir, G., Aillerie, M. "A single-phase photovoltaic microinverter topology based on boost converter", Przeglad Elektrotechniczny, 95(4), pp. 215–217, 2019. https://doi.org/10.15199/48.2019.04.40

[5] Desingu, S., Mouttou, A. "FOPID Controller Design and Implementation for High Gain Quadratic Boost Switched Capacitor Converter", Periodica Polytechnica Electrical Engineering and Computer Science, 64(4), pp. 382–391, 2020. https://doi.org/10.3311/PPee.15783

[6] Ismeil, M., Hussein, S. H., Nasrallah, M. "Micro Inverter Grid Connected for PV Application Based on SEPIC Differential Inverter", SVU-International Journal of Engineering Sciences and Applications, 5(1), pp. 1–12, 2024. https://doi.org/10.21608/svusrc.2023.224660.1142

[7] Janardhan, K., Mittal, A., Ojha, A. "Performance investigation of stand-alone solar photovoltaic system with single phase micro multilevel inverter", Energy Reports, 6, pp. 2044–2055, 2020. https://doi.org/10.1016/j.egyr.2020.07.006

[8] Diyoke, G. C., Ogbuka, C. U., Nwosu, C. M. "A novel control DC-DC-AC buck converter for single phase capacitor-start-run induction motor drives", Advances in Electrical and Electronic Engineering, 17(2), pp. 87–95, 2019. https://doi.org/10.15598/aeee.v17i2.2904

[9] Ghribi, M. E. B., Ternifi, Z. E. T., Bachir, G., Aillerie, M. "Buck-Based Photovoltaic Microinverter Coupled to a Discharge Circuit", Majlesi Journal of Electrical Engineering, 18(1), pp. 323–333, 2024. https://doi.org/10.30486/mjee.2024.1992377.1189

[10] Yaqoob, S. J., Raham, J. K., Sadiq, H. A. "Analysis and Simulation of Current-source Flyback Inverter with Efficient BCM Control Strategy", WSEAS Transactions on Electronics, 12, pp. 132–140, 2021. https://doi.org/10.37394/232017.2021.12.18

[11] Ghribi, M. E. B., Ternifi, Z. E. T., Bachir, G., Aillerie, M. "Micro-Inverter Based on Symmetrical Boost-Discharge Topology for Photovoltaic Energy Source", Advances in Electrical and Electronic Engineering, 21(4), pp. 305–313, 2023. https://doi.org/10.15598/aeee.v21i4.5212

[12] Wang, L., Liu, C., Fang, J. "Design of a Single-Stage Transformerless Buck–Boost Inverter for Electric Vehicle Chargers", Applied Sciences, 12(13), 6705, 2022. https://doi.org/10.3390/app12136705

[13] Danyali, S., Aghaei, O., Shirkhani, M., Aazami, R., Tavoosi, J., Mohammadzadeh, A., Mosavi, A. "A New Model Predictive Control Method for Buck-Boost Inverter-Based Photovoltaic Systems", Sustainability, 14(18), 11731, 2022. https://doi.org/10.3390/su141811731

[14] Lyapunov, A. M. "The general problem of the stability of motion", International Journal of Control, 55(3), pp. 531–534, 1992. https://doi.org/10.1080/00207179208934253

[15] Ateş, M., Laribi, S. "New results on the global asymptotic stability of certain nonlinear RLC circuits", Turkish Journal of Electrical Engineering and Computer Sciences, 26(1), pp. 434–441, 2018. https://doi.org/10.3906/elk-1612-100

[16] Ullah, N., Al Ahmadi, A. "Variable structure back-stepping control of two-stage three phase grid connected pv inverter", Periodica Polytechnica Electrical Engineering and Computer Science, 64(3), pp. 239–246, 2020. https://doi.org/10.3311/PPee.15412

[17] Khan, T. I., Luu, H. T., Szamel, L. "Deadbeat Predictive Control Method for 4-leg Inverters", Periodica Polytechnica Electrical Engineering and Computer Science, 67(1), pp. 70–82, 2023. https://doi.org/10.3311/PPee.20981